Sensors & Actuators: B. Chemical 440 (2025) 137886

Contents lists available at ScienceDirect

Sensors and Actuators: B. Chemical

journal homepage: www.elsevier.com/locate/snb

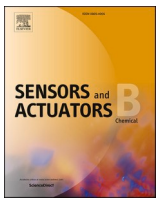

High-specificity near-infrared fluorescent probe for chymotrypsin imaging: Innovative diagnostic tool for pancreatic diseases

Jingkang Li [a], Mo Ma [a,c], Chen Zhao [a], Lanyun Zhang [a], Wanqi Li [a], Pinyi Ma [a,*], Shan Jiao [b,*], Daqian Song [a,*]

[a] College of Chemistry, Jilin Province Research Center for Engineering and Technology of Spectral Analytical Instruments, Jilin University, Qianjin Street 2699, Changchun 130012, China
[b] Hospital of Stomatology, Jilin University, Qinghua Road 1500, Changchun 130021, China
[c] School of Pharmacy, Jilin University, Qianjin Street 2699, Changchun 130012, China

ARTICLE INFO

Keywords:
Fluorescent Probe
Chymotrypsin
Nile red
Pancreatitis
Pancreatic cancer

ABSTRACT

Pancreatic diseases are closely linked with the abnormal activity of various proteases, including chymotrypsin. Currently, probes specifically designed for the detection of chymotrypsin in pancreatic disorders are unavailable. In this study, we developed a highly specific and sensitive fluorescent probe for the detection of chymotrypsin activity to enable precise diagnosis of pancreatic diseases. The probe was incorporated with Nile red as the fluorescent moiety and 4-bromobutanoyl as the recognition and quenching group to facilitate a "fluorescence switch" response upon enzymatic cleavage. The probe had high specificity and sensitivity to chymotrypsin, which remained unaffected in the presence of 52 biological interferents. It had a linear detection range of 0.1–0.75 μg/mL and a limit of detection of 0.0203 μg/mL, indicative of superior analytical performance. Cellular assays showed that the probe could effectively distinguish between normal pancreatic cells and tumor cells. Furthermore, the applications of the probe in pancreatitis models revealed its capability to accurately differentiate between normal tissue, chronic pancreatitis, and acute pancreatitis and to provide robust support for real-time imaging and disease progression monitoring. Subsequent *in vivo* experiments further validated the probe's diagnostic efficacy, highlighting its potential in the diagnosis of pancreatic diseases. These findings provide a solid foundation for developing molecular tools for early diagnosis and therapeutic monitoring of pancreatic disorders, demonstrating its significant potential in clinical diagnostics and precision medicine.

1. Introduction

Pancreatic diseases, including acute pancreatitis (AP) [1–3], chronic pancreatitis (CP) [4–6], and pancreatic cancer (PC) [7], present significant diagnostic and therapeutic challenges due to their complex pathophysiological mechanisms and the absence of distinct early symptoms [8,9]. Accurate early diagnosis is crucial for effectively managing disease progression and improving patient prognosis [10–14]. Among various potential biomarkers, chymotrypsin (CHT)—a serine protease secreted by the pancreas—has emerged as a focal point of research owing to its pivotal role in pancreatic function regulation and its involvement in pathological states [15–17]. Abnormal CHT activity is closely associated with the onset and progression of pancreatic diseases, positioning it as a crucial target for diagnostic applications [18,19].

In recent years, organic small-molecule fluorescent probes have gained popularity as essential tools for studying disease mechanisms and facilitating early diagnosis, owing to their high sensitivity, selectivity, and ability to monitor biological processes in real-time in complex biological systems [20–26]. These probes can be used directly visualize enzymatic activities to provide crucial insights into disease states [27–30]. In 2017, Yang et al. developed a fluorescent probe using 4-bromobutanoyl as the recognition moiety for chymotrypsin [31]. This is the first CHT-responsive small molecule probe that is not a peptide recognition group. Compared to traditional peptide-based substrates, this probe is significantly advantageous in terms of structural simplicity and sensitivity. Despite the widespread application of the 4-bromobutanoyl recognition group [32–34], studies on CHT-based fluorescent probes for diagnosing deep-seated tumors remain limited.

To address this gap, Lin et al. introduced a dual-modal 3D-PA/NIRF fluorescent probe activated by CHT for precise tumor imaging [35]. The

* Corresponding authors.
E-mail addresses: mapinyi@jlu.edu.cn (P. Ma), jiaoshan@jlu.edu.cn (S. Jiao), songdq@jlu.edu.cn (D. Song).

https://doi.org/10.1016/j.snb.2025.137886
Received 14 February 2025; Received in revised form 16 April 2025; Accepted 27 April 2025
Available online 28 April 2025

probe generates intense near-infrared fluorescence signals at tumor sites, markedly improving the contrast between tumors and the surrounding healthy tissues. For these reasons, the probe was able to delineate the boundaries of P815 tumors, acting as vital support for anatomical analysis. This imaging strategy demonstrates potential as a tool for guiding clinical treatments and evaluating therapeutic efficacy. However, the applications of CHT probe in pancreatic diseases have not been explored. Given the critical role of CHT in pancreatic pathology, developing high-specificity fluorescent probes to differentiate between diseased and normal pancreatic states remains a challenge. Successful construction of such probes as novel tools for the early diagnosis pancreatic diseases is, therefore, crucial.

In this study, we constructed a fluorescent probe NR-CHT for the specific detection of CHT using 4-bromobutanoyl as the recognition moiety and hydroxy Nile red (NR-OH), a highly efficient fluorescent dye, as the foundational fluorophore. The fluorescence of the probe is effectively quenched upon binding. *In vitro* experiments demonstrated that the NR-CHT probe was responsive to CHT and had excellent specificity and sensitivity. It was able to successfully detect CHT activity. Cellular assays were conducted to further investigate the application of the NR-CHT probe in pancreatic diseases, revealing that it can sensitively detect changes in endogenous CHT activity within cells. Subsequently, pancreatic disease cell models were established and used in an experiment to study the expression of CHT in different pathological states at the cellular level. The results indicated that the NR-CHT probe effectively distinguished between normal pancreatic cells and pathological pancreatic cells. Furthermore, *in vivo* imaging experiments demonstrated that the NR-CHT probe generated strong near-infrared fluorescence signals at tumor sites, leading to significantly enhanced contrast between tumors and the surrounding healthy tissues. Additionally, in mouse models of acute and chronic pancreatitis, the NR-CHT probe exhibited outstanding capabilities in effectively differentiating between chronic and acute pancreatitis.

2. Experimental methods

2.1. Materials and equipment

Detailed information regarding reagents and instruments used in this study can be found in the Supplementary Material. The synthesis route is illustrated in Fig. 1.

Synthesis of NR-OH. Compound 1 was synthesized following a reported method [36]. Specifically, Compound 1 (165 mg, 1 mmol) and 2, 6-dihydroxynaphthalene (240 mg, 1.5 mmol) were dissolved in 2 mL of DMF, and the mixture was stirred overnight at 150°C. After cooling to room temperature, 40 mL of saturated salt water and ethyl acetate were added to extract the organic layer. The organic phase was then purified by silica gel column chromatography using a mixture containing ethyl acetate and petroleum ether at a ratio of 3:1 as the eluent. The compound NR-OH was obtained as a dark red solid with a 20 % yield. ^{1}H NMR (600 MHz, DMSO-d_6) δ 10.40 (s, 1 H), 7.96 (d, J = 8.6 Hz, 1 H), 7.87 (d, J = 2.5 Hz, 1 H), 7.56 (d, J = 9.0 Hz, 1 H), 7.08 (dd, J = 8.5, 2.5 Hz, 1 H), 6.78 (dd, J = 9.1, 2.7 Hz, 1 H), 6.62 (d, J = 2.7 Hz, 1 H), 6.14 (s, 1 H), 3.48 (q, J = 7.1 Hz, 4 H), 1.16 (t, J = 7.0 Hz, 6 H). ^{13}C NMR (151 MHz, DMSO-d_6) δ 182.02, 161.06, 152.05, 151.13, 146.86, 139.18, 134.21, 131.27, 127.92, 124.32, 124.31, 118.81, 110.35, 108.57, 104.55, 96.50, 44.88, 12.92. MS data (LC-ESI-MS, m/z) for $C_{20}H_{19}N_2O_3^+$ $[M+H]^+$: calculated, 335.1390; found: 335.1393. (Figures S1-S3)

Synthesis of NR-CHT. NR-OH (100 mg) was dissolved in anhydrous acetonitrile, and the solution was cooled in an ice bath. After 100 μL of triethylamine was added, the solution was continuously stirred for 5 min. While maintaining in an ice bath, 100 μL of 4-bromobutyryl chloride was added dropwise to the mixture. After that, the temperature was gradually raised to room temperature, and the stirring was continued for 1 hour. The solvent was then evaporated under reduced pressure to concentrate the reaction mixture. The mixture was purified by silica gel column chromatography using a mixture containing ethyl acetate and petroleum ether at a ratio of 1:1.The desired product, NR-CHT, was obtained as a purple solid with a 56 % yield. ^{1}H NMR (600 MHz, DMSO-d_6) δ 8.26 – 8.18 (m, 1 H), 8.16 (dd, J = 8.6, 7.2 Hz, 1 H), 7.61 (dd, J = 9.1, 4.6 Hz, 1 H), 7.48 (d, J = 8.4 Hz, 1 H), 6.84 (dd, J = 9.1, 2.7 Hz, 1 H), 6.66 (t, J = 2.6 Hz, 1 H), 6.27 (d, J = 3.4 Hz, 1 H), 3.79 (t, J = 6.5 Hz, 1 H), 3.51 (q, J = 7.0 Hz, 4 H), 3.36 (s, 2 H), 2.85 (d, J = 7.2 Hz, 1 H), 2.16 (p, J = 6.8 Hz, 2 H), 1.17 (t, J = 7.0 Hz, 6 H). ^{13}C NMR (151 MHz, DMSO-d_6) δ 181.56, 153.31, 152.56, 151.55, 147.06, 133.58, 131.49, 129.13, 127.50, 124.72, 116.44, 110.93, 104.78, 96.48, 44.98, 27.78, 12.93, 9.73. MS data (LC-ESI-MS, m/z) for $C_{24}H_{24}BrN_2O_4^+$ $[M+H]^+$: calculated, 483.0914; found: 483.0905. (Figures S4-S6)

2.2. Detection of CHT in solution

A 1 mM stock solution of the fluorescent probe NR-CHT was prepared in DMSO. The following parameters were systematically optimized:

Reaction time. Reaction mixtures containing 0.7 μg/mL or 1 μg/mL CHT and 10 μM NR-CHT were prepared in phosphate-buffered saline (PBS, 10 mM, pH 7.4). These mixtures were incubated at 37℃ for varying times (0, 10, 20, 30, 40, 60, 80, 100, 120, and 150 min). The optimal reaction time was determined based on changes in fluorescence signals.

pH level. PBS solutions with different pH values (4, 5, 6, 7, 7.4, 8, 9, 10, and 11) were prepared. Reaction mixtures containing 1 μg/mL CHT and 10 μM NR-CHT were incubated at 37℃ for 120 min. The pH yielding the highest fluorescence signal was identified as the optimal pH.

Reaction temperature. Mixtures containing 1 μg/mL CHT and 10 μM NR-CHT were prepared in PBS and incubated at various temperatures (25℃, 30℃, 37℃, 40℃, and 45℃) for 120 min. The temperature that yielded the highest reaction efficiency was identified as the optimal temperature.

Probe selectivity. Reaction mixtures containing 10 μM NR-CHT were dissolved in PBS and incubated at 37℃ for 120 min. Fluorescence spectroscopy was employed to assess the selectivity to CHT of the probe. Specific concentrations of the assay and the method of its preparation are detailed in the Supplementary Material.

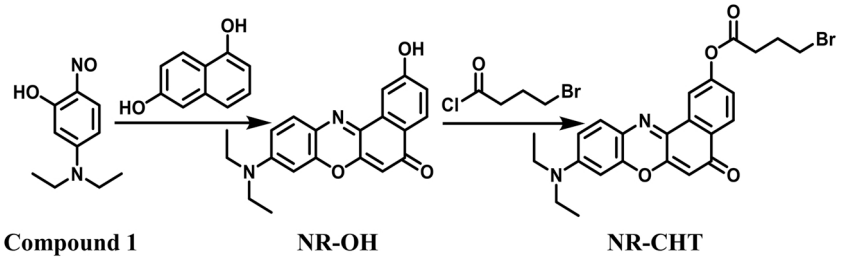

Fig. 1. Synthetic route of probe NR-OH and NR-CHT.

Enzyme kinetic parameters. NR-CHT probe solutions at varying concentrations (1, 2, 3, 4, 5, 7, 10, 13, 16, 20, and 30 μM) were prepared in 10 mM PBS buffer, pH 7.4. Each solution was supplemented with 2 μg/mL CHT. Fluorescence intensity was recorded every 3 min at an excitation wavelength of 580 nm and an emission wavelength of 690 nm every 3 min over a period of 30 min. Initial reaction rates were calculated by fitting the fluorescence intensity change curves within the linear response range of the reaction. The kinetic parameters of the hydrolysis reaction were determined using both the Michaelis-Menten and Lineweaver-Burk equations.

2.3. Establishment of cell model

To investigate the dynamic changes in CHT activity at the cellular level and evaluate the imaging performance of the fluorescent probe NR-CHT, normal pancreatic (AR42J) and pancreatic cancer (Panc-2) cell lines were utilized as models for systematic cell imaging experiments. Prior to imaging, cells were cultured in glass-bottom culture dishes under conditions (37℃ and 5 % CO_2) for 24 h. Imaging experiments were conducted using an IX-73 inverted fluorescence microscope at an excitation wavelength of 580 nm to ensure high-sensitivity signal acquisition.

Dynamic changes in CHT activity. Cells were incubated with 10 μM NR-CHT, and fluorescence signals were recorded at different time points (0, 10, 20, 30, and 60 min) using time-lapse imaging to analyze dynamic changes in fluorescence intensity.

Evaluation of NR-CHT imaging performance in different pathological states. The experimental groups were categorized as follows: (1) Control group: Normal pancreatic cells incubated with 10 μM NR-CHT for 60 min; (2) Disease model group: Pancreatic cancer cells incubated with 10 μM NR-CHT for 60 min; (3) Acute pancreatitis model [37]: Normal pancreatic cells treated with 500 μM L-arginine for 1 h, followed by incubation with 10 μM NR-CHT; (4) Chronic pancreatitis model: Normal pancreatic cells subjected to repeated treatments with 100 μM L-arginine for 3 days to establish a chronic pancreatitis model, followed by incubation with 10 μM NR-CHT.; and (5) Inhibition group [35]: Normal pancreatic cells pre-treated with 1 mg/mL PMSF (phenylmethylsulfonyl fluoride) before incubation with 10 μM NR-CHT. Fluorescence signals from different experimental groups were analyzed by fluorescence microscopy imaging techniques to assess the imaging performance of the NR-CHT probe under various pathological conditions and its sensitivity to changes in CHT activity.

2.4. Establishment of mice model

All animal experiments were conducted in strict accordance with the ethical guidelines established by the Animal Ethics Committee of Jilin University (IACUC) and were approved by the ethics review board (License No.: SY202409009). BALB/c-nu mice were used to establish a series of pancreatic disease models as outlined below:

Pancreatic cancer mouse model. A suspension of 1×10^7 Panc-2 cells in 300 μL PBS was subcutaneously injected into the dorsal region of mice. Fourteen days post-injection, and these tumor-bearing mice were used for subsequent experiments.

Acute pancreatitis mouse model. Acute pancreatitis was induced by intraperitoneal injection of L-arginine following the methods reported in the literature [37]. Mice received three evenly spaced intraperitoneal injections of L-arginine (4.5 g/kg) within 1 h, with a 30-minute waiting period following the final injection.

Chronic pancreatitis mouse model. Chronic pancreatitis was established by daily intraperitoneal injections of L-arginine (1.0 g/kg) for 14 consecutive days.

Acute pancreatitis treatment model. In this study, we established an acute pancreatitis model using the L-arginine induction method, as described in the literature [37]. After the model was induced, the treatment group received intravenous administration of ustekin, an endogenous trypsin inhibitor isolated and purified from the urine of healthy adults. Ustekin has been clinically used for the treatment of acute pancreatitis, and its clinical efficacy has been demonstrated in multicenter studies conducted in Japan, India, and China [38]. The specific dosing regimen consisted of two intravenous doses of 100 μL ustekin solution (10,000 U/mL), administered 6 h apart on the first day, followed by a single dose every two days for the subsequent 6 days.

Probe administration and imaging. Pancreatic Cancer Models: 10 μM NR-CHT fluorescent probe solution (200 μL) was *in situ* injected into the pancreatic cancer model mice. Inflammatory Models: The probe was administered via tail vein injection. Mice were maintained under isoflurane anesthesia throughout the imaging. Fluorescence imaging data were collected every 5 min using a small animal imaging system. Control group mice underwent identical injection and imaging procedures to minimize non-specific factors affecting the results and ensure data reliability.

3. Results and discussion

3.1. Probe design and mechanism verification

In this study, we designed and synthesized an enzyme-responsive fluorescent probe, NR-CHT, utilizing NR-OH as the fluorophore for the specific detection of CHT. NR-OH possessed excellent photophysical properties, including a high fluorescence quantum yield, long emission wavelength, and robust photostability. These properties are significantly advantageous to the detection in biological systems. Structurally, NR-OH is linked to the recognition moiety, 4-bromobutanoyl, via an ester bond. In the absence of chymotrypsin, the fluorescence of the fluorophore is quenched, resulting in weak fluorescence signals. However, upon interaction with chymotrypsin, the enzyme selectively recognizes and hydrolyzes the 4-bromobutanoyl moiety, releasing the quenching group. This structural change triggers a significant fluorescence enhancement, generating an "Off-On" fluorescence response. The specificity of this mechanism is attributed to the high affinity and selective recognition between the probe's recognition moiety and chymotrypsin, effectively minimizing non-specific interference from other proteases.

To further validate the hydrolysis reaction and investigate the mechanism of NR-CHT in sensing chymotrypsin, we employed multiple analytical techniques, including high-performance liquid chromatography-mass spectrometry (HPLC-MS), theoretical calculations, and molecular docking simulations. As illustrated in Fig. 2A, the introduction of CHT resulted in a significant decrease in the mass peak intensity of NR-CHT (m/z 483.0904), along with the simultaneous appearance of the NR-OH mass peak (m/z 335.1347). Subsequent HPLC analysis (Fig. 2B) revealed characteristic peaks at retention times of 3.17 min and 5.45 min corresponding to NR-CHT and NR-OH, respectively. These findings support the proposed sensing mechanism, confirming that CHT-mediated hydrolysis of NR-CHT produces NR-OH. Theoretical calculations were conducted to provide additional insights. As depicted in Fig. 2 C, the electrostatic potential analysis revealed that NR-OH had a more pronounced charge transfer capability compared to NR-CHT. This indicates that the hydrolysis by CHT enhances the intramolecular charge transfer (ICT) effect, resulting in a significant fluorescence signal enhancement. Additionally, molecular docking experiments were performed to demonstrate the probe's effective targeting of the CHT recognition site. As shown in Fig. 2D, NR-CHT was observed to enter the active center of CHT, where it interacted with multiple amino acid residues. These interactions exhibited a low binding energy of −7.4 kcal/mol, indicating a strong binding affinity between NR-CHT and CHT. Collectively, these data validate the probe's mechanism of action, highlighting its ability to effectively bind and interact with the target enzyme, thereby enabling effective fluorescence-based sensing of CHT activity.

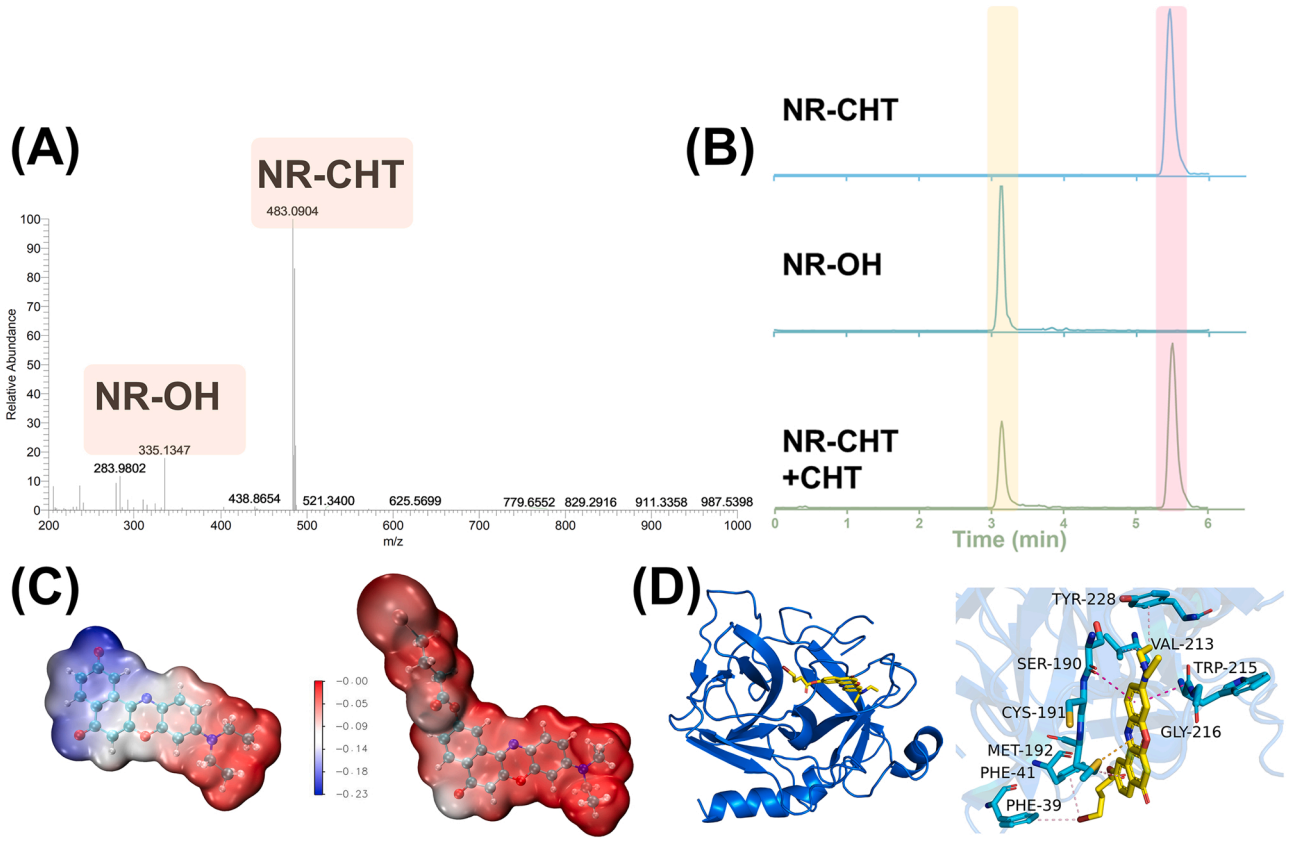

Fig. 2. (A) MS result of the reaction solution (B) HPLC-MS result of the reaction solution (C) Electrostatic potential distribution of NR-OH and NR-CHT (D) Molecular docking simulation for the binding between NR-CHT and CHT.

3.2. Optimization of in vitro test conditions

To evaluate the analytical performance of NR-CHT, we systematically optimized various testing conditions, including reaction time, pH, and temperature.

The reaction time was first optimized. As shown in Fig. 3B, in the presence of CHT, the fluorescence intensity of the probe (λ_{em} = 690 nm) gradually increased with increasing reaction time, reaching a maximum value at 120 min before plateauing. To further verify the stability of the probes and fluorescent dyes, we conducted time-course experiments. As shown in Figure S7, the fluorescence intensity remained stable during the 150 min monitoring period, with fluctuations kept within a narrow range. No significant attenuation or abnormal fluctuations were observed, indicating good stability. Thus, 120 min was selected as the optimal reaction time to ensure the enzymatic reaction reached completion.

The results also demonstrated that the fluorescence signal remained stable at the temperature range of 30–45℃, suggesting its suitability for physiological conditions (Figure S8A). Similarly, the fluorescence signal was stable at around pH 7.4, which aligns with physiological environments (Figure S8B). Given that CHT typically catalyzes reactions under physiological conditions, we observed a significant decrease in enzymatic activity, along with the fluorescence signal intensity, when the pH exceeded 8, which is indicative of reduced catalytic efficiency at higher pH levels. Based on these findings, the optimal experimental conditions were as follows: a reaction time of 120 min, pH 7.4, and a temperature of 37 ℃.

Under the optimal conditions, we further examined the linear relationship between the fluorescence intensity (λ_{em} = 690 nm) of NR-CHT and the concentration of CHT. The results indicated a clear correlation between fluorescence signal intensity and CHT concentration. Specifically, upon excitation at 580 nm, the fluorescence intensity at 690 nm of NR-CHT (10 μM) progressively increased with increasing CHT concentrations from 0 to 2 μg/mL (Fig. 3 C), reaching saturation at approximately 2 μg/mL. A strong linear relationship between FL intensity and CHT concentration was observed within the concentration range of 0.1–0.75 μg/mL (Fig. 3D). The limit of detection (LOD) was calculated to be 0.0203 μg/mL, which is a low detection threshold.

The selectivity of NR-CHT to CHT was evaluated in the presence of various potential interferents, including amino acids, metal ions, anions, thiols, ROS and RNS (Fig. 3E). The probe showed high selectivity for CHT, with negligible interference from the tested substances. Subsequently, we investigated the enzyme kinetics between NR-CHT and CHT using Michaelis-Menten and Lineweaver-Burk plots (Figures S8C and Figure S8D). The maximum reaction velocity (V_{max}) was determined to be 16.404 μM min^{-1}, and the Michaelis constant (K_m) was 2.943 μM. These kinetic parameters reflect a high affinity and efficient catalytic interaction between NR-CHT and CHT.

These results not only validate the high sensitivity of the NR-CHT probe but also highlight its excellent performance across a wide concentration range and superior detection accuracy. The linear correlation and low LOD (0.0203 μg/mL) also highlight its potential for the quantitative detection of CHT activity in biomedical applications, particularly in the early diagnosis and monitoring of disease progression.

3.3. Fluorescence imaging of cellular CHT

The cytotoxicity of NR-CHT was evaluated using the CCK-8 assay. The results showed that cell viability remained above 90 % across all tested concentrations (Figure S9A and Figure S9B), demonstrating that NR-CHT had minimal cytotoxicity. Hemolysis assays further demonstrated the low hemolysis rate of NR-CHT, confirming its high biocompatibility (Figure S9C).

Microscopic imaging revealed that NR-CHT was rapidly uptaken by

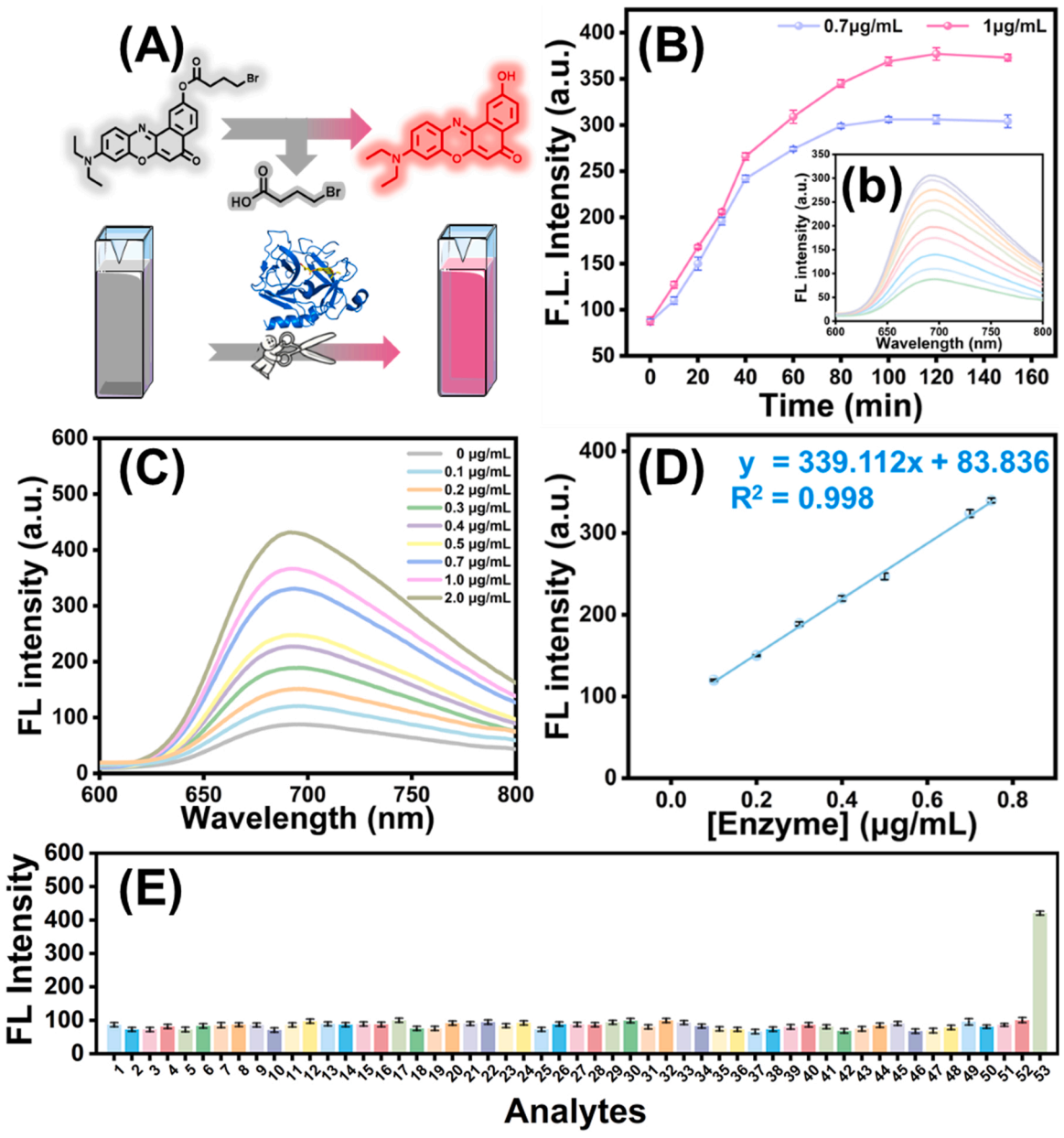

Fig. 3. (A) Schematic diagram of enzymatic hydrolysis. (B) Temperature-dependent fluorescence intensity (λ_{emmax} = 690 nm) of 10 μM NR-CHT in the presence or absence of CHT. (b represents the plot at CHT=1 μg/mL). (C) Fluorescence spectra (λ_{emmax} = 690 nm) a solution consisting of 10 μM NR-CHT and 0–2 μg/mL CHT. (D) Linear relationship between fluorescence intensity at 690 nm and CHT concentrations (0.1–0.75 μg/mL). (E) Fluorescence intensity of 10 μM NR-CHT in the presence of various interferents (1 mM, unless otherwise stated). 1–12: different anions (Br^-, $ONOO^-$, Cl^-, ClO_4^-, CN^-, F^-, $H_2PO_4^-$, HPO_4^{2-}, HSO_4^-, I^-, SCN^-, SO_3^{2-}); 13–30: cations (Ag^+, Al^{3+}, Ba^{2+}, Ca^{2+}, Cd^{2+}, Co^{2+}, Cu^{2+}, Fe^{2+}, Fe^{3+}, Hg^{2+}, K^+, Li^+, Mg^{2+}, Mn^{2+}, Na^+, Ni^{2+}, Pb^{2+}, Zn^{2+}); 31–48: amino acids and proteins (Asp, Cys, GSH, Hcy, His, Ser, Tyr, Val, Phe, Ala, Met, Gly, Glu, Arg, Lys, Leu, NAC, Thr); 49–52: ROS (H_2O_2, O_2^-, $ONOO^-$) and RNS (NO) ; 53: 1 μg/mL CHT were added to the solution as a disturbance group.

cells, as indicated by the progressive increase in fluorescence intensity until reaching its peak at 60 min (Fig. 4). This suggests that NR-CHT has a rapid response time in intracellular imaging. Subsequently, inhibitor experiments confirmed the specificity of NR-CHT to endogenous CHT. In control experiments, the fluorescence intensity of pancreatic cells pre-treated with PMSF (a serine protease inhibitor) followed by incubation with the probe was significantly reduced (Fig. 5). This indicates that the fluorescence enhancement in the cells is due to interaction between endogenous CHT and NR-CHT. According to the literature [39], CHT is a serine protease secreted by the pancreas and highly abundant in pancreatic cells. The overexpression of chymotrypsin may facilitate the provision of necessary nutrients for tumor cells; as a result, abnormal secretion of chymotrypsin is often observed in proliferating tumor cells [40]. As shown in Fig. 5, fluorescence signals of normal pancreatic cells and pancreatic cancer cells were distinctly different, with the latter displaying significantly brighter fluorescence, which is consistent with the hypothesis. This demonstrates that the probe is effective in distinguishing between normal and cancerous cells.

We established models of acute pancreatitis (AP) and chronic pancreatitis (CP) and subsequently performed imaging of the models using the probe. According to the literature [39], chymotrypsin in acute pancreatitis is prematurely activated and excessively secreted, leading to inflammation. In contrast, chronic pancreatitis involves different pathological mechanisms, including cellular damage that reduces enzyme synthesis and secretion [39,41]. As illustrated in Fig. 5, AP cells exhibited more pronounced fluorescence signals compared to CP cells,

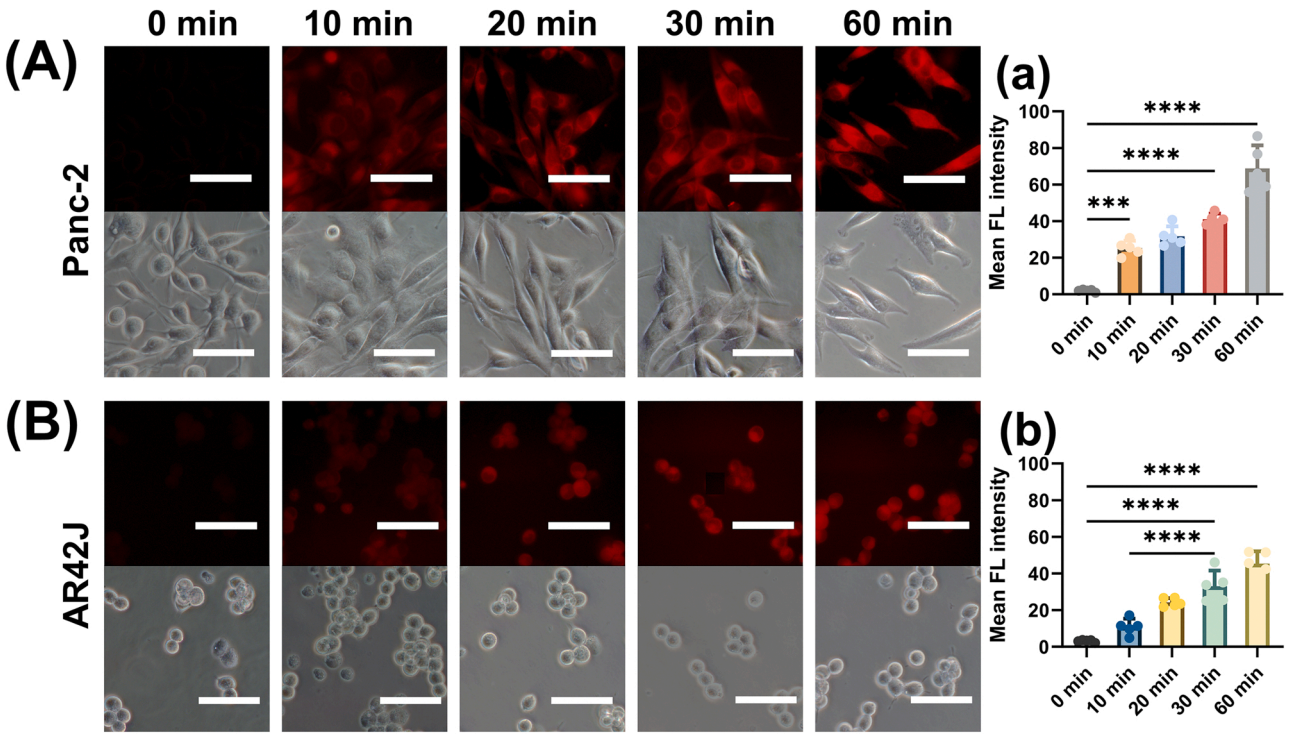

Fig. 4. Fluorescence images of pancreatic and pancreatitis cells (A: pancreatic cancer cells, B: normal pancreatic cell). (a) Mean fluorescence intensity of cells in (A) (****$P < 0.0001$, data analyses were performed on independent samples with equal variances; data are means ± SD; n = 3). (b) Mean fluorescence intensity of cells in (B) (****$P < 0.0001$, data analyses were performed on independent samples with equal variances; data are means ± SD; n = 3). Scale bar = 50 μm.

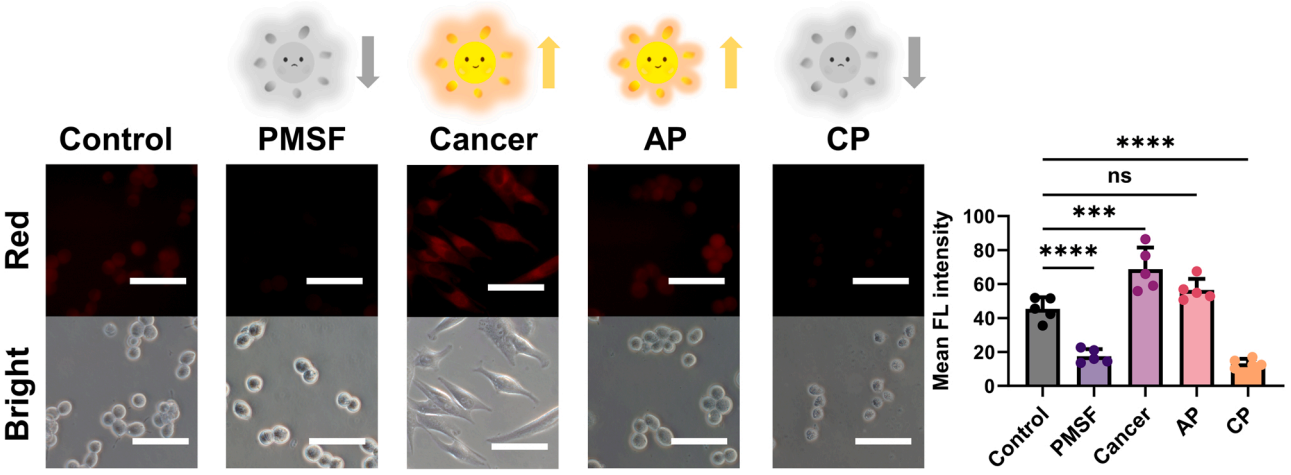

Fig. 5. Fluorescence images of pancreatic cell models (Control: normal pancreatic cell AR42J, PMSF: inhibitor of CHT, Cancer: pancreatic cancer cell Panc-2, AP: acute pancreatitis model, CP: chronic pancreatitis model) (****$P < 0.0001$, data analyses were performed on independent samples with equal variances; data are means ± SD; n = 5). Scale bar = 50 μm.

which exhibited markedly reduced signals. These results confirm that CHT is overexpressed in acute pancreatitis cells but underexpressed in chronic pancreatitis, consistent with the hypothesized mechanism. In summary, NR-CHT is a potent tool for monitoring CHT and the pathological status of pancreatic cells.

3.4. *In vivo fluorescence imaging-guided surgery*

Building on the promising results from cellular experiments, the application of NR-CHT was extended to *in vivo* bioimaging. The above studies have demonstrated that the probe can effectively differentiate between normal and tumor cells, as well as between AP and CP cells. CHT, a serine protease secreted by the pancreas, plays a crucial role in pancreatic function and pathological states. In pancreatic cancer, the high proliferation and metabolic demands of tumor cells may drive abnormal secretion [42]. This elevated activity is closely linked to the metabolic requirement of cancer cells and their aggressive growth characteristics.

To investigate the pancreatic cancer mouse model, we first established an orthotopic tumor in mice. The probe was injected *in situ*, and fluorescence imaging was performed over time. As fluorescence signals progressively intensified, a prominent signal was observed within 30 min post-injection (Figure S10). This demonstrates that NR-CHT is an excellent imaging probe for imaging pancreatic cancer. We then

explored the applicability of NR-CHT in guiding tumor resection. By uniformly spraying the probe onto the tumor site, we observed that the fluorescence signal was first stable but became more prominent after 30 min. Guided by this fluorescence signal, the tumor was surgically excised. The fluorescence signal of the excised tumor was stable, whereas that of areas outside the tumor was minimal. This confirms that as directed by the probe's fluorescence, the cancerous region was completely removed (Fig. 6B). To characterize the tumor margins in mice, hematoxylin and eosin (HE) staining was performed on the excised tumors. The staining revealed that minimal normal tissue remained at the tumor margins, demonstrating the precision and efficacy of NR-CHT probe-guided tumor resection (Figure S11A).

3.5. *In vivo fluorescence imaging of mice with pancreatitis*

To explore more functions of the probe beyond imaging malignant tumors, we examined the expression of CHT in pancreatitis models *in vivo*. We established both AP and CP mouse models, Then HE staining was used to verify the model. As is shown in Figure S11B, HE staining results showed that pancreatic acinus showed different degrees of cell necrosis, the space in the tissue was enlarged, and the interstitial was loose. The above results demonstrated the successful establishment of an acute pancreatitis model. To confirm the successful establishment of the chronic pancreatitis model, histological staining of the pancreas was conducted. HE staining results showed steatosis, local hemorrhage of pancreas and loss of acinar cells, which proved the successful establishment of chronic pancreatitis (Figure S11C). The probe was then injected through the tail vein and then imaged with a small animal imaging system. For in vivo toxicity evaluation, we measured serum and whole blood biochemical indices in both healthy mice and inflammation model mice. Liver function analysis revealed that total bilirubin levels remained within the normal physiological range (1.7–15 μM), with no significant fluctuations observed after probe injection. Additionally, alkaline phosphatase (ALP) activity, a key marker of hepatobiliary function, remained stable within the reference range (62–209 U/L), and no significant differences were detected between groups after probe administration (Figure S12). Blood routine tests showed that the red blood cell (RBC) count and red blood cell pressure (HCT) were elevated

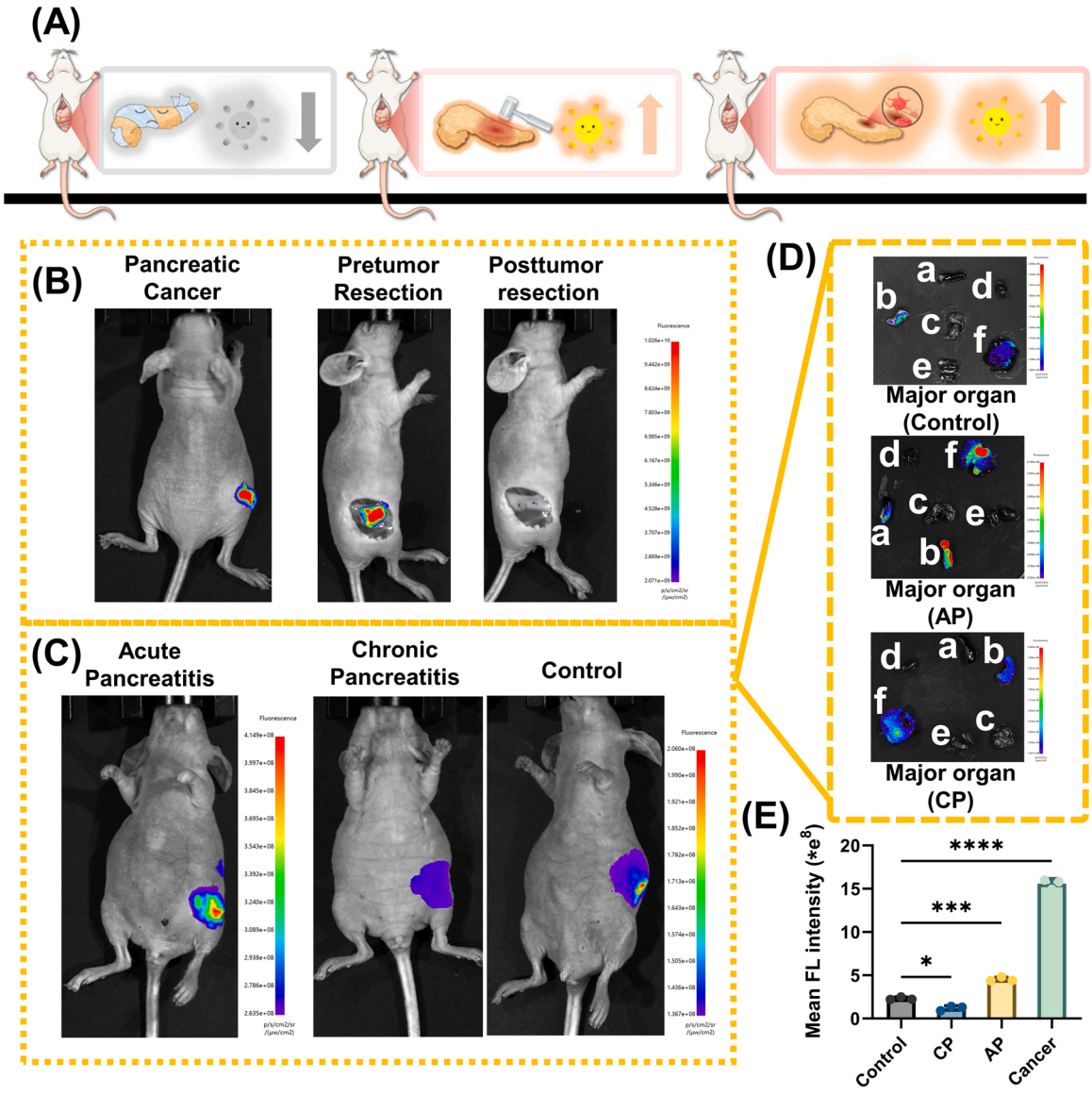

Fig. 6. (A) Schematic diagram showing the diagnostic imaging of pancreatic disease model. (B) Fluorescence images of tumor and tumor resection. (C) Fluorescence images of inflammatory mice and control mice. (D) Organ anatomy of mice with acute pancreatitis and chronic pancreatitis (a: spleen, b: pancreas, c: lung, d: heart, e: kidney f: liver). (E) Quantitative comparison of imaging data (****$P < 0.0001$, data analyses were performed on independent samples with equal variances; data are means ± SD; n = 3).

in the inflammation model group, consistent with the expected hemoconcentration effect of acute inflammation. Importantly, no significant differences in RBC or HCT levels were observed between the probe-treated and control groups, indicating that the probe did not affect these parameters (Figure S13). These results confirm that the NR-CHT probe exhibits low biotoxicity and good biocompatibility. According to the literature [43], acute inflammation causes pancreatic acinar cells to release precursors such as chymotrypsinogen. During inflammation, chymotrypsinogen in pancreatic tissue is prematurely activated to chymotrypsin, resulting in high expression levels of chymotrypsin in AP mice. As shown in Fig. 6 C, the area adjacent to the pancreas exhibited a significant fluorescence signal. Upon dissection, the pancreas clearly exhibited strong fluorescence (Fig. 6D). To confirm the successful establishment of the acute pancreatitis model, histological staining of the pancreas was performed. In acute inflammation, CHT is overexpressed, which is consistent with our hypothesis. We also established a chronic pancreatitis model, which differs from acute inflammation. Chronic pancreatitis involves long-term repetitive inflammation and fibrosis, leading to gradual fibrotic changes in normal tissues that significantly impair the secretory capacity of the pancreas. As depicted in Fig. 6D, we injected the probe into both normal mice and chronic pancreatitis mice. The area near the pancreas in normal mice exhibited prominent fluorescence, whereas chronic pancreatitis mice exhibited weaker fluorescence. Upon dissection, fluorescence in the pancreases of chronic pancreatitis mice was markedly reduced compared to normal mice. To further verify the above results, we measured the enzyme levels in the pancreatic tissues of mice using an ELISA kit, as detailed in the Supplementary Material. As shown in Figures S14B and C, the enzyme level in the control group was 540 μg/L. In mice with chronic pancreatitis, the enzyme level significantly decreased to 67.98 μg/L, consistent with the observed pancreatic damage and impaired enzyme synthesis and secretion due to prolonged chronic inflammation. In contrast, mice with acute pancreatitis exhibited an enzyme level of 1640.86 μg/L, substantially higher than that of the control group, further supporting the experimental findings.

To further validate the sensitivity of the probe in diagnosing pancreatic diseases, ustekin treatment was applied to the established pancreatitis model. Ustekin is a peptide drug clinically used for both acute and chronic recurrent pancreatitis [38]. As shown in Figure S15, the acute pancreatitis model exhibited a strong fluorescence signal, while the treatment group displayed a significantly reduced fluorescence signal, similar to that of the control group. This indicates that the NR-CHT probe was highly sensitive in monitoring the therapeutic process of pancreatitis. To further validate the therapeutic effect of the drug, histological analysis was performed using hematoxylin and eosin (HE) staining. As shown in Figure S16A, pancreatic tissue from the acute pancreatitis group displayed prominent inflammation. In contrast, tissue from the treatment group (Figure S16B) showed signs of inflammation reversal, closely resembling the blank control group (Figure S16C). These results further confirm the effectiveness of the drug treatment and highlight the sensitivity of the NR-CHT probe in monitoring the therapeutic outcome.

To investigate the metabolic time of the fluorescent probe, *in vivo* fluorescence imaging was performed over a 6-hour period following the injection of the probe into mice. As shown in Figure S17, within the first hour, the probe quickly accumulated in the pancreatic region, exhibiting a strong fluorescence signal, indicating effective enrichment in the tissue. Over time, the fluorescence signal progressively shifted to the liver, suggesting that the probe was metabolized predominantly by the liver. By the fourth hour, the fluorescence signal had substantially decreased, and by the fifth hour, significant fluorescence was observed in the metabolites, confirming the probe's metabolism. By the sixth hour, the fluorescence signal was almost undetectable in vivo. To validate these observations, we conducted in vitro fluorescence imaging of the major organs, which showed no significant residual fluorescence. These findings confirm that the probe possesses excellent in vivo metabolic properties, is efficiently cleared post-imaging, and demonstrates strong biological safety and application potential. Thus, NR-CHT proves to be an effective tool for monitoring CHT activity and evaluating the pathological status of pancreatic cells *in vivo*.

4. Conclusion

We successfully developed NR-CHT, a high-specificity and high-sensitivity CHT-targeting near-infrared fluorescent probe. The design of NR-CHT involved the incorporation of 4-bromobutyryl as the CHT-recognition moiety to enable high-precision detection of CHT activity in complex biological environments. Comprehensive *in vitro* and *in vivo* experiments validated the probe's performance, revealing that it had a low limit of detection, a wide linear detection range, and exceptional selectivity, sensitivity, and stability. Under pathological conditions, NR-CHT exhibited a significantly enhanced fluorescence signal and was employed to affirm the clinical relevance of CHT as a potential biomarker for pancreatic diseases. The NR-CHT probe was able to distinguish normal pancreatic tissue and pancreatic tumor tissue and effectively differentiated between chronic pancreatitis and acute pancreatitis. This demonstrates its versatility in diagnosing various pancreatic conditions. Overall, these findings highlight the crucial role of NR-CHT in disease diagnostics, showcasing it as an innovative tool for the early detection and diagnosis of pancreatic disorders.

CRediT authorship contribution statement

Ma Pinyi: Writing – review & editing, Software, Project administration, Data curation. **Li Wanqi:** Investigation. **Zhang Lanyun:** Investigation. **Zhao Chen:** Investigation, Data curation. **Ma Mo:** Investigation, Data curation. **Li Jingkang:** Writing – original draft, Validation, Investigation, Data curation, Conceptualization. **Song Daqian:** Supervision, Resources, Project administration, Funding acquisition. **Jiao Shan:** Writing – review & editing, Investigation, Data curation.

Declaration of Competing Interest

The authors declare that they have no known competing financial interests or personal relationships that could have appeared to influence the work reported in this paper.

Acknowledgements

This work was supported by the National Natural Science Foundation of China (22004046 and 22074052) and the Science and Technology Developing Foundation of Jilin Province of China (20210204130YY).

Appendix A. Supporting information

Supplementary data associated with this article can be found in the online version at doi:10.1016/j.snb.2025.137886.

Data availability

Data will be made available on request.

References

[1] L. Boxhoorn, R.P. Voermans, S.A. Bouwense, M.J. Bruno, R.C. Verdonk, M. A. Boermeester, et al., Acute pancreatitis, Lancet 396 (2020) 726–734.
[2] P. Szatmary, T. Grammatikopoulos, W.H. Cai, W. Huang, R. Mukherjee, C. Halloran, et al., Acute Pancreatitis: Diagnosis and Treatment, Drugs 82 (2022) 1251–1276.
[3] Y.H. Gao, N.N. Mi, W.X. Wu, Y.X. Zhao, F.Z. Fan, W.W. Liao, et al., Transfer of inflammatory mitochondria via extracellular vesicles from M1 macrophages induces ferroptosis of pancreatic beta cells in acute pancreatitis, J. Extra Vesicles 13 (2024) e12410.

[4] G. Beyer, A. Habtezion, J. Werner, M.M. Lerch, J. Mayerle, Chronic pancreatitis, Lancet 396 (2020) 499–512.
[5] J. Kleeff, D.C. Whitcomb, T. Shimosegawa, I. Esposito, M.M. Lerch, T. Gress, et al., Chronic pancreatitis, Nat. Rev. Dis. Prim. 3 (2017) 17060.
[6] V.K. Singh, D. Yadav, P.K. Garg, Diagnosis and Management of Chronic Pancreatitis A Review, JAMA 322 (2019) 2422–2434.
[7] Z.I. Hu, E.M. O'Reilly, Therapeutic developments in pancreatic cancer, Nat. Rev. Gastroenterol. Hepatol. 21 (2024) 7–24.
[8] M.A. Mederos, H.A. Reber, M.D. Girgis, Acute Pancreatitis: A Review, JAMA 325 (2021) 382–390.
[9] X.J. Liu, M.M. Song, T. Hou, F. Li, Label-Free Homogeneous Electroanalytical Platform for Pesticide Detection Based on Acetylcholinesterase-Mediated DNA Conformational Switch Integrated with Rolling Circle Amplification, Acs Sens. 2 (2017) 562–568.
[10] H. Wang, X.T. Zhang, P. Li, F. Huang, T.C. Xiu, H.T. Wang, et al., Prediction of Early Atherosclerotic Plaques Using a Sequence-Activated Fluorescence Probe for the Simultaneous Detection of γ-Glutamyl Transpeptidase and Hypobromous Acid, Angew. Chem. Int Ed. 63 (2024) e202315861.
[11] L.L. Xu, M. Ma, J.K. Li, D.F. Dai, D.J. Gao, P.Y. Ma, et al., Exploration of aminopeptidase N as new biomarker for early diagnosis of thyroid cancer, Biosens. Bioelectron. 244 (2024) 115808.
[12] Y. Liu, Y.C. Yao, J.H. Sha, G.L. Liang, X.B. Sun, Dual-Locked Enzyme-Activatable Fluorescence Probes for Precise Bioimaging, ACS Biomater. Sci. Eng. 115554 (2025).
[13] Q. Zhang, H.W. Yang, J. Gao, R.D. Lv, K. Zheng, P. Zhang, et al., NIR Fluorescence Strategy for the Early Diagnosis of Melanoma Liver Metastasis Based on the Cascade Reaction of Two Specific Bioenzymes, Anal. Chem. (2025) 3125–3135.
[14] P.P. Gai, C.C. Gu, T. Hou, F. Li, Ultrasensitive Self-Powered Aptasensor Based on Enzyme Biofuel Cell and DNA Bioconjugate: A Facile and Powerful Tool for Antibiotic Residue Detection, Anal. Chem. 89 (2017) 2163–2169.
[15] O.G. Famutimi, V.G. Adebiyi, B.G. Akinmolu, O.V. Dada, I.O. Adewale, Trypsin, chymotrypsin and elastase in health and disease, Future J. Pharm. Sci. 10 (2024) 126.
[16] J.F. Chang, H.Y. Li, T. Hou, F. Li, Paper-based fluorescent sensor for rapid naked-eye detection of acetylcholinesterase activity and organophosphorus pesticides with high sensitivity and selectivity, Biosens. Bioelectron. 86 (2016) 971–977.
[17] W.J. Chen, H.H. Liu, F.X. Song, L.T. Xin, Q. Zhang, P. Zhang, et al., pH-Switched Near-Infrared Fluorescent Strategy for Ratiometric Detection of ONOO- in Lysosomes and Precise Imaging of Oxidative Stress in Rheumatoid Arthritis, Anal. Chem. 95 (2023) 1301–1308.
[18] Y. Qu, Z.S. Xu, J.M. Wang, W. Liu, A. Iqbal, K. Iqbal, et al., Strong red fluorescent probe for detecting chymotrypsin activity in vivo and in vitro, Sens Actuators B Chem. 382 (2023) 133552.
[19] M.L. Zhang, Y.Q. Wang, N. Li, D.Q. Zhu, F. Li, Specific detection of fungicide thiophanate-methyl: A smartphone colorimetric sensor based on target-regulated oxidase-like activity of copper-doped carbon nanozyme, Biosens. Bioelectron. 237 (2023) 115554.
[20] M. Ma, S.Q. Zhang, J.K. Li, L.H. Zhao, D.Q. Song, P.Y. Ma, et al., Carboxylesterase 2-based fluorescent probe with large Stokes shift for differentiating colitis from bowel cancer, Sens Actuators B Chem. 426 (2025) 137057.
[21] S.Q. Zhang, M. Ma, J.K. Li, L.L. Xu, P.Y. Ma, H. Han, et al., Neutrophil elastase specific fluorescent probe for early diagnosis of thyroiditis via serum sample testing and fluorescence imaging, Sens Actuators B Chem. 423 (2025) 136736.
[22] Y.L. Chen, W.Q. Li, S. Li, L. Liu, J. Yang, P. Wang, Sulfone-Embedded NIR Fluorophore with Large Stokes Shift for Monitoring Viscosity Changes during NAFLD-Induced Ferroptosis, Acs Sens. 10 (2024) 398–406.
[23] Z.W. Zhao, W. Xiang, W.T. Guo, B.D. Wang, A Dual-Channel Fluorescence Probe for Early Diagnosis and Treatment Monitoring of Acute Kidney Injury by Detecting HOCl and Cys with Different Fluorescence Signals, Anal. Chem. 97 (2025) 2127–2135.
[24] J.K. Li, M. Ma, Z.M. Zhang, L.L. Xu, B. Yang, Q.P. Diao, et al., A novel carboxylesterase 2-targeted fluorescent probe with cholic acid as a recognition group for early diagnosis of drug- and environment-related liver diseases, J. Hazard Mater. 480 (2024) 135966.
[25] L.Z. Xu, Q. Zhang, X. Wang, W.Y. Lin, Biomedical applications of NIR-II organic small molecule fluorescent probes in different organs, Coord. Chem. Rev. 519 (2024) 216122.
[26] H. Wang, X.T. Zhang, T.C. Xiu, H.T. Wang, P. Li, B. Tang, Fluorescence probes for sensing and imaging within Golgi apparatus, Coord. Chem. Rev. 502 (2024) 215618.
[27] M. Deng, P.P. Wang, Z.B. Zhai, Y. Liu, D. Cheng, L.W. He, et al., A Triple-Responsive and Dual-NIR Emissive Fluorescence Probe for Precise Cancer Imaging and Therapy by Activating Pyroptosis Pathway, Anal. Chem. (2025) 2998–3008.
[28] Y.C. Hu, X. Gao, J.L. Ma, Z.C. Shangguan, L.L. Chen, G.X. Zhang, et al., New AIE Emitters from the Unexpected Boron Tribromide/Boron Trichloride-mediated Cyclization Reaction and Application for Fluorescence Imaging of Lipid Droplets, Aggregate (2025).
[29] H. Wang, J.J. Guo, T.C. Xiu, Y. Tang, P. Li, W. Zhang, et al., H2O2 accumulation promoting internalization of ox-LDL in early atherosclerosis revealed via a synergistic dual-functional NIR fluorescence probe, Chem. Sci. 16 (2024) 345–353.
[30] F. Zhang, Y.A. Song, H.Z. Yan, H.F. Yang, Z.H. Liu, Z.F. Li, et al., A lighting up NIR fluorescent sensing assay for norepinephrine and its application in the imaging of depressed mice brain, Sens Actuators B Chem. 417 (2024) 136182.
[31] L. Wu, S.H. Yang, H. Xiong, J.Q. Yang, J. Guo, W.C. Yang, et al., Nonpeptide-Based Small-Molecule Probe for Fluorogenic and Chromogenic Detection of Chymotrypsin, Anal. Chem. 89 (2017) 3687–3693.
[32] J.M. Wang, Z.D. Teng, T. Cao, J. Qian, L. Zheng, Y.P. Cao, et al., Turn-on visible and ratiometric near-infrared fluorescent probes for distinction endogenous esterases and chymotrypsins in live cells, Sens Actuators B Chem. 306 (2020) 127567.
[33] S. Mu, Y.X. Xu, Y.T. Zhang, X.M. Guo, J. Li, Y.L. Wang, et al., A non-peptide NIR fluorescent probe for detection of chymotrypsin and its imaging application, J. Mater. Chem. B 7 (2019) 2974–2980.
[34] Y.P. Chen, J. Cao, X.X. Jiang, Z.Z. Pan, N.Y. Fu, A sensitive ratiometric fluorescence probe for chymotrypsin activity and inhibitor screening, Sens Actuators B Chem. 273 (2018) 204–210.
[35] Y.P. Zhao, X. Zou, X. Liang, L. Huang, W.Y. Lin, A non-peptide chymotrypsin activatable probe for 3D-photoacoustic and NIR fluorogenic imaging of deep tumor, Sens Actuators B Chem. 382 (2023) 133553.
[36] J.K. Li, M. Ma, S.Q. Zhang, W.P. Dong, P.Y. Ma, Z.W. Zhang, et al., Cholesterol esterase-responsive near-infrared fluorescent probe for precise imaging of atherosclerosis, Sens Actuators B Chem. 427 (2025) 137150.
[37] Q.Y. Yin, W.J. Yang, Y.Z. Huang, Y.D. Zhu, J.M. Ding, B.G. Li, et al., Near-infrared imaging of acute pancreatitis with a pancreatic lipase-monitoring fluorescence probe, Sens Actuators B Chem. 414 (2024) 135970.
[38] J. Hey-Hadavi, P. Velisetty, S. Mhatre, Trends and recent developments in pharmacotherapy of acute pancreatitis, Postgrad. Med. 135 (2023) 334–344.
[39] A. Saluja, V. Dudeja, R. Dawra, R.P. Sah, Early Intra-Acinar Events in Pathogenesis of Pancreatitis, Gastroenterology 156 (2019) 1979–1993.
[40] L. Liu, H.J. Xiong, W.Y. Sun, T.Y. Wang, Y.H. Wang, J. Wang, et al., Chymotrypsin etched ultrasmall gold nanoclusters for dual response diagnosis and deeply penetrated chemodynamic therapy of pancreatic cancer, Sens Actuators B Chem. 413 (2024) 135880.
[41] D.L. Conwell, L.S. Lee, D. Yadav, D.S. Longnecker, F.H. Miller, K.J. Mortele, et al., American Pancreatic Association Practice Guidelines in Chronic Pancreatitis Evidence-Based Report on Diagnostic Guidelines, Pancreas 43 (2014) 1143–1162.
[42] A. Jermusyk, J. Zhong, K.E. Connelly, N. Gordon, S. Perera, E. Abdolalizadeh, et al., A 584 bp deletion in CTRB2 inhibits chymotrypsin B2 activity and secretion and confers risk of pancreatic cancer, Am. J. Hum. Genet 108 (2021) 1852–1865.
[43] A. Geisz, Z. Janscó, B.C. Németh, E. Hegyi, M. Sahin-Tóth, Natural single-nucleotide deletion in chymotrypsinogen C gene increases severity of secretagogue-induced pancreatitis in C57BL/6 mice, Jci Insight 4 (2019) e129717.

Jingkang Li is currently a PhD student in College of Chemistry, Jilin University. His interest is spectral analysis.

Mo Ma is currently a PhD student in School of Pharmacy, Jilin University. His interest is spectral analysis.

Chen Zhao is currently a PhD student in College of Chemistry, Jilin University. Her interest is spectral analysis.

Lanyun Zhang is currently a master degree student in College of Chemistry, Jilin University. Her interest is spectral analysis.

Wanqi Li is currently a master degree student in College of Chemistry, Jilin University. Her interest is spectral analysis.

Pinyi Ma received his doctor's degree from College of Chemistry, Jilin University in 2017 and he is an associate professor in that school. His research area is spectral analysis.

Shan Jiao gained her doctor's degree from College of Chemistry, Jilin University in 2020 and she is an associate chief physician in the endodontics department of stomatological hospital, Jilin University. Her research areas are stomatology and optical sensing.

Daqian Song received his doctor's degree from College of Chemistry, Jilin University in 2003 and he is a professor in that school. His research areas are spectral and chromatography analysis.